Fragility Curves and Loss Estimation for Traditional Timber-framed Masonry Buildings in Lefkas, Greece

Leonidas Alexandros S. Kouris[1] and Andreas J. Kappos[2]

Abstract The 2003 earthquake in the Greek island of Lefkas, has revived the interest for the local anti-seismic technique based on the use of timber-framed masonry, whose adequate performance during the earthquake revealed the merits of this rather sophisticated, albeit traditional, construction. A key feature of the Lefkas structures is their dual structural system. The secondary system is activated once the ground storey stone masonry piers of the primary system (which includes timber-framed masonry in all storeys) fail. In this regard, two different structural models are presented herein to simulate the response of each system. A macro-model based on nonlinear (NL) strut elements and point plastic hinges is intended to model the timber-framed masonry. NL analyses are carried out for one, two and three storey buildings , which represent the most common cases in Lefkas. Furthermore, an investigation is carried out regarding the foundation of the buildings resting on soft alluvial deposits. Pushover curves are derived from the NL analyses of the buildings and are then converted to capacity curves using the characteristics of the predominant mode. On these curves four damage states (slight damage, moderate damage, heavy damage, and collapse) are defined on the basis of criteria related to the actual response of the building. Then, fragility curves in terms of spectral displacement are generated, adopting a log-normal statistical distribution. These curves are converted into PGA values using a selected response spectrum. Utilising these fragility curves a seismic loss scenario for the 2003 Lefkas earthquake is developed for the timber-framed masonry stock of Lefkas city.

Keywords: Timber-framed masonry buildings, Lefkas traditional buildings, fragility curves in terms of S_d, fragility curves in terms of PGA, loss assessment, capacity curves**.**

1. INTRODUCTION

Recent earthquakes and several experimental campaigns on timber-framed masonry walls have shown that timber-framed masonry buildings possess a good displacement capacity. The seismic capacity of structures is better understood and related to the displacement capacity rather than the strength capacity (Moehle 1992; Kowalsky et al. 1995; Kappos and Stefanidou 2010). Therefore, timber-framed masonry structures can withstand catastrophic earthquakes avoiding collapse as the Lefkas 2003 earthquake has shown (Karababa and Guthrie 2007).

[1] Leonidas Alexandros S. Kouris
Aristotle University of Thessaloniki, 541 24 Thessaloniki, Greece
e-mail: l.a.kouris@gmail.com
Present address: Rose School, IUSS Pavia, 27100, Pavia, Italy.
[2] Andreas J. Kappos
City University of London, EC1V OHB London, UK
e-mail: Andreas.Kappos.1@city.ac.uk

Timber-framed masonry is a traditional structural system that in seismic areas has proved to effectively resist earthquakes (Kouris and Kappos 2009; Vieux-Champagne et al. 2014). It is well known that unreinforced masonry buildings in general cannot resist strong earthquakes; their high vulnerability, documented during several recent earthquakes (see for example Indirli et al. 2013; Kouris et al. 2010) originates from low tensile, and hence shear, strength and the low ductility of its components resulting in poor seismic performance with local out-of-plane mechanisms before the in-plane capacity of its members is reached. The performance of vulnerable unreinforced masonry can be enhanced when a combination of wood and masonry is applied which can provide the necessary seismic capacity. Buildings made in some form of timber-framed masonry are found in ancient Greece from the Bronze Age (16^{th} century B.C.) and ever since they have a continuous history and a fairly widespread presence.

An important evolution of the structural system of timber-framed masonry is the inclusion of diagonal timber members in the frame. This diagonally braced timber-framed masonry was used as an anti-seismic construction at least from the 18^{th} century in seismic-prone areas as well as in regions without considerable seismic risk, for resisting wind actions or, when the buildings were founded on soft soils, differential settlements. Indeed, in the latter case the diagonally braced timber-framed masonry system provides a light and effective structure to resist diagonal tension caused by soil settlement. Timber-framed masonry buildings of the early modern times or even the late Renaissance are found in abundance apart from the high seismicity areas globally (Vieux-Champagne et al. 2014), also in low or negligible seismic hazard areas such as Central Europe (Kappos and Kouris 2008) and Nordic countries (Copani 2007). **Figure 1** shows a building situated in Ameland, Holland in the North Sea which is an area with soft thin sandstone layers (De Jong et al. 2014) and suffers mainly from soil subsidence. A few diagonals are sufficient to provide the necessary strength against differential settlement and lateral wind loads.

A very advanced from the structural engineering point of view timber-framed masonry construction appears in an earthquake prone area, the Lefkas Island, in the Ionian Sea (western part of Greece). This structural system was produced by local builders in the region at least since the 17^{th} century A.D.; it is reported that after the destructive earthquake that hit Lefkas in 1825 the local authorities decided to rebuild collapsed buildings of the island using this system which had performed very well (Touliatos 1995). Erecting such a structural system which comprises wood and masonry in harmonious proportions is a challenging task that could be properly carried out only by highly-skilled builders.

Figure 1. Timber-framed building in Ameland, Holland.

The development of this structural system, which to some extent follows the principles of displacement-based design (a recent trend in earthquake engineering), has strongly benefitted from the experience gained by frequent, yet of moderate intensity, earthquakes in the area, that permitted observations and inspired improvements in the course of time. In its historical context, the system is a pioneer construction and this is a key reason why it has been listed as a monument of world heritage by the United Nations (1993). However, construction of these traditional buildings came to an abrupt end during the last century since modern structures overwhelmingly prevailed; hence nowadays most of them date back at least a century ago. Timber-framed masonry buildings have received a considerable amount of attention by architects and archaeologists. On the other hand very little has been done so far to assess their seismic capacity and vulnerability.

To predict the response of structures to future earthquakes it is necessary to generate fragility curves that will be used to develop loss estimation scenarios based on the seismic hazard of a region (Vamvatsikos et al. 2010a). Empirical fragility curves have been published for timber-framed masonry buildings using data from the 2003 Lefkas earthquake. After this earthquake a detailed survey of damage and collapse has been carried out in two phases by the local Departments for Seismic Restoration (TAS) in the municipalities of Lefkas. The first phase was the rapid evaluation with a colour tag characterisation (green-yellow-red), while the second was more detailed and was completed after four months. Processing this data, Karababa (2007) generated fragility curves for the timber-framed masonry buildings of Lefkas. The main disadvantage of these empirical curves, apart from being presented in terms of a parameterless seismic intensity scale rather than PGA values, is that they are based on a single event. To this end it is necessary to enhance the existing set of fragility curves with new ones based on analytical results. This chapter first describes the structural details related to the seismic behaviour of this dual system and a methodology for their modelling; then it

presents the results from the analysis, and finally assesse their seismic vulnerability with the development of analytical fragility curves and a loss scenario for the 2003 Lefkas earthquake.

2. MODELLING OF SEISMIC RESPONSE

2.1 Description of the structural system

The origin of the timber-framed masonry (TFM) system of Lefkas has been lost after the 1825 strong earthquake (Papazachos et al. 1997; Rondoyanni et al. 2012) which destroyed the greatest part of the city (Stamatelos 1870). Constructions which could be a predecessor of the dual system have probably collapsed or been demolished, and were replaced by the anti-seismic dual system (Touliatos 1995). The dual system has performed better than all other structures and hence, it has been selected as the appropriate construction type for Lefkas by the authorities (Vintzileou and Touliatos 2005). Specific regulations define the details of the construction techniques; among others the regulations specify the materials to be used in the construction, the thickness and the height of the ground storey walls.

The structures in Lefkas can be distinguished in two broad categories (Porphyrios 1971): (i) the pure timber-framed masonry system when the building is a single-storey house and (ii) the dual system when the building is a multi-storey (usually two or three storeys) construction. The ordinary single-storey TFM buildings hereafter are referred to as *pure* timber-framed masonry buildings to distinguish them from the latter buildings with a *dual* system.

As already mentioned, multi-storey dual timber-framed masonry buildings in Lefkas have an unreinforced masonry ground storey. In most case cases this is an unreinforced stone masonry wall whose usually calcareous limestone stones are extracted from local quarries or those of the neighbouring Epirus coast (Karababa 2007; Touliatos and Gante1995). The height of the ground storey is on average 3 m and its width may vary from 0.6 to 1.0 m. The external façade is made of ashlar-work while the internal one is made of roughly dressed and worked stones or rubble walls in irregular courses. Upper storeys are made in timber-framed masonry.

Timber-framed masonry of the upper storeys consists of timber elements forming a 3D timber frame and masonry infills. Timber sections are on average 10 (±2) cm square. The timber frame has spans that vary from around 1.0 up to 2.2 m. Diagonal members join opposite corners but sometimes one of them may miss or be halved. An important feature of TFM is the use of curved timber elements to stiffen the connection of timber posts to beams. These angles are L-shaped for single-sided connections (Figure 2) or T-shaped for double-sided connections. It is clear that local builders had comprehended the substantial lateral load capacity of timber elements and tried to exploit them as much as possible.

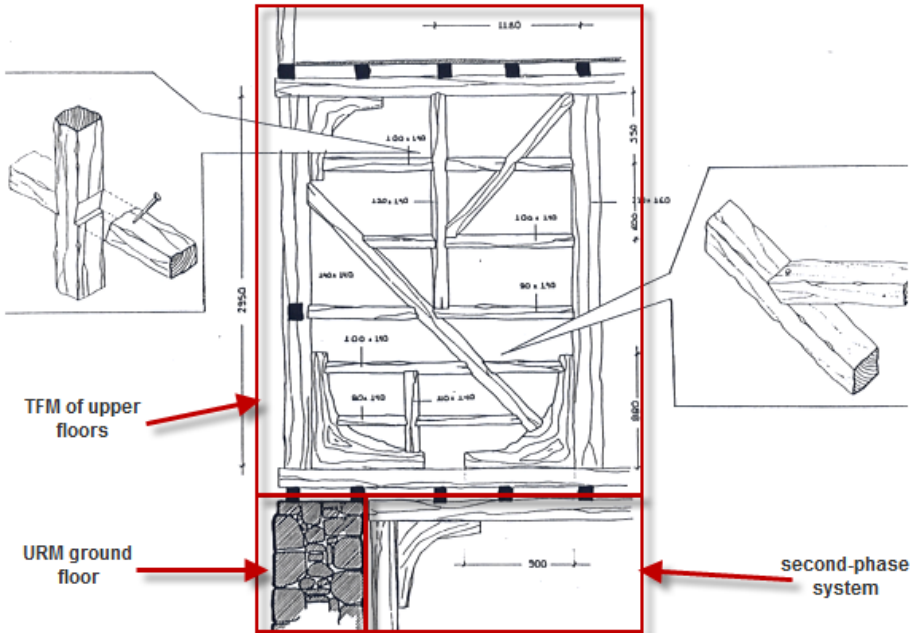

Figure 2. Connection of timber-framed masonry superstructure with the unreinforced masonry ground storey and the secondary system (Touliatos and Gante 1995).

The connection of timber beams and timber posts and the connection of the diagonals are materialised through T-shaped lap carpentry joint and iron nails (Figure 3a). In some cases the connection of the diagonals is not through carpentry joints but rather one diagonal is compact (i.e. one solid element) while the second consists of two separate parts (two elements) as shown in Figure 3b, i.e. joint by splices (Vintzileou 2011). This detailing is typically associated with lower quality of construction. The T-shaped lap carpentry connection strengthened by L or T-shaped angles is close to a monolithic one, i.e. moment-resisting connection.

Nevertheless, the unique structural feature of the Lefkas buildings is their dual system. In fact, apart from the unreinforced masonry ground storey there is a secondary structural system on the internal side of the walls comprised of timber posts (Apostolopoulos and Sotiropoulos 2008). Normally, to every pier corresponds a single timber post a few centimetres apart the walls (**Figure 2**). This small distance of the timber posts from the walls results from the plinth foundation of the posts which is usually on a compact massive stone appropriately curved and usually equipped with thin metal plates that clamp the base of the column (**Figure 3**c). These timber posts are connected to the beams, as well as the timber-framed masonry walls, of the upper storey. Hence, the beams of the floors and the timber-framed masonry walls are supported by both the primary and the secondary system. This sophisticated connection is realised by embedding floor beams into the unreinforced masonry ground storey walls and at the same time joining them to the timber columns of the secondary system.

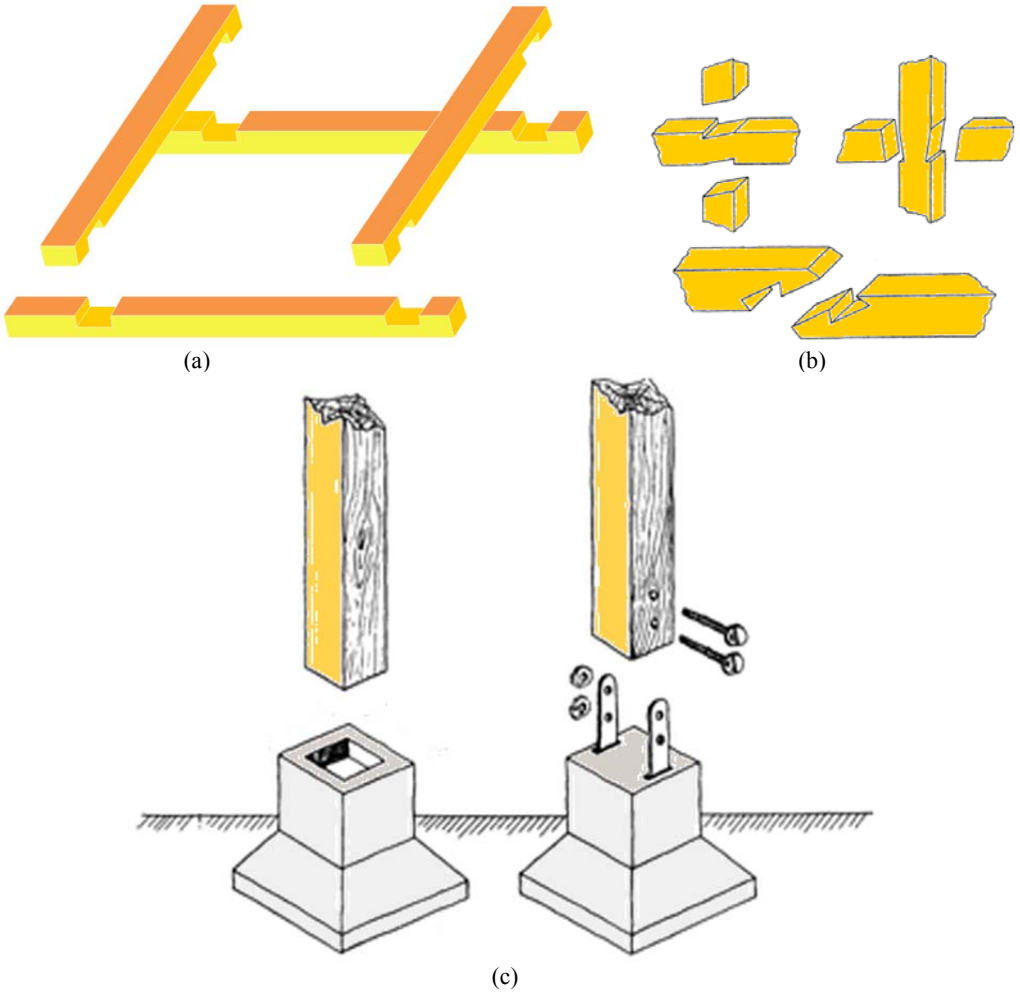

Figure 3. Timber connections: (a) between beams and posts (T-shaped lap joint), (b) splices for longitudinal members (Porphyrios 1971), and (c) stone foundations of timber posts of the secondary system (Porphyrios 1971).

Timber columns are not subjected to gravity loads under service conditions of the building and support to the upper floors gravity loads is provided solely by the primary system (i.e. the unreinforced masonry ground storey). During an earthquake, if its intensity is that high as to drive the unreinforced masonry ground storey walls to partial or full collapse the secondary system will be activated. Due to the much higher deformability of the timber columns compared to the URM walls, this secondary system has displacement reserves able to accommodate the increased displacement demand of the earthquakes, at the expense, of course, of significant damage. Collapse of the URM walls of the ground storey may be classified as 'severe damage' state. Consequently, the building will be able to avoid collapse, but damage will be high or possibly irreparable due to permanent displacements after the earthquake; however, adequate life safety is ensured.

2.2 Geometry and materials of the typical building

A timber-framed masonry building with the previously described dual system situated in the central square of Lefkas city called the 'Berykiou' building (**Figure 4**) is selected for further analysis. This building has geometrical and mechanical characteristics that are typical of the timber-framed masonry structures found in the island.

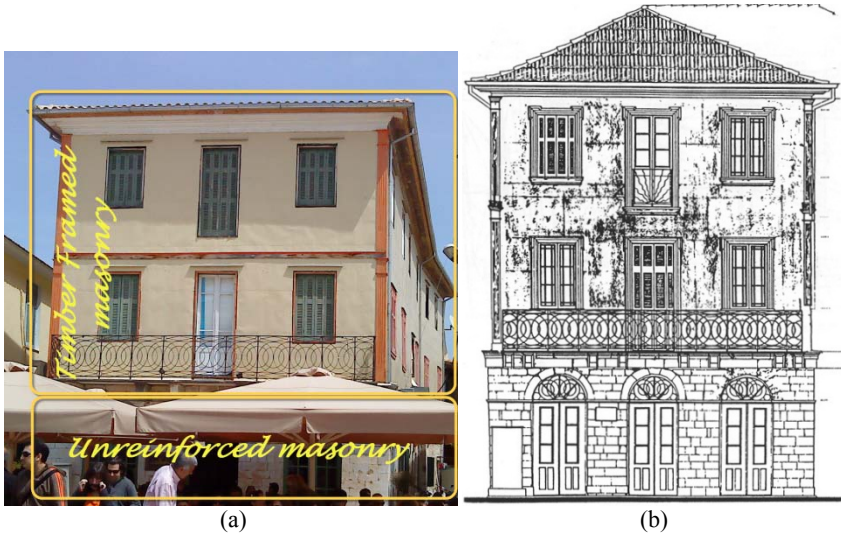

(a) (b)

Figure 4. The 'Berykiou' building: (a) the façade and, (b) architectural survey (by Touliatos and Gante 1995) in the central square of the Lefkas city.

The building comprises of two parts (**Figure 4**a): (i) its ground storey is made of limestone with stonework texture in courses and the thickness of the walls is 0.8 m (**Figure 4**b), while (ii) the upper storeys are made in timber-framed masonry. **Figure 5** presents the basic geometry of the building façade. Timber-framed masonry of the upper storeys is covered with thin galvanized iron sheathing for their protection against weathering and dry rot considering the vicinity to the sea. Timber-framed panels of the upper storeys are assumed to have a configuration consisting of two diagonals as illustrated in **Figure 5**b. A previously developed model for timber-framed masonry with two diagonal braces is utilised (Kouris et al. 2014). During the rapid post-damage survey after the Lefkas 2003 earthquake the building was characterized 'Green', i.e. low damage, in the tagging system (Red-Yellow-Green) presenting an adequate performance.

Gravity load emanating from the timber frame of the upper storeys timber-framed masonry is supported by only the ground storey unreinforced masonry under service conditions). However, the timber posts of the secondary system shown in **Figure 5**b are also connected to the timber frame but they will receive load only during earthquake failure of the ground storey. The eccentric connection of the timber post (secondary system) to the timber frame (primary system) is realized through iron anchors (Figure 2).

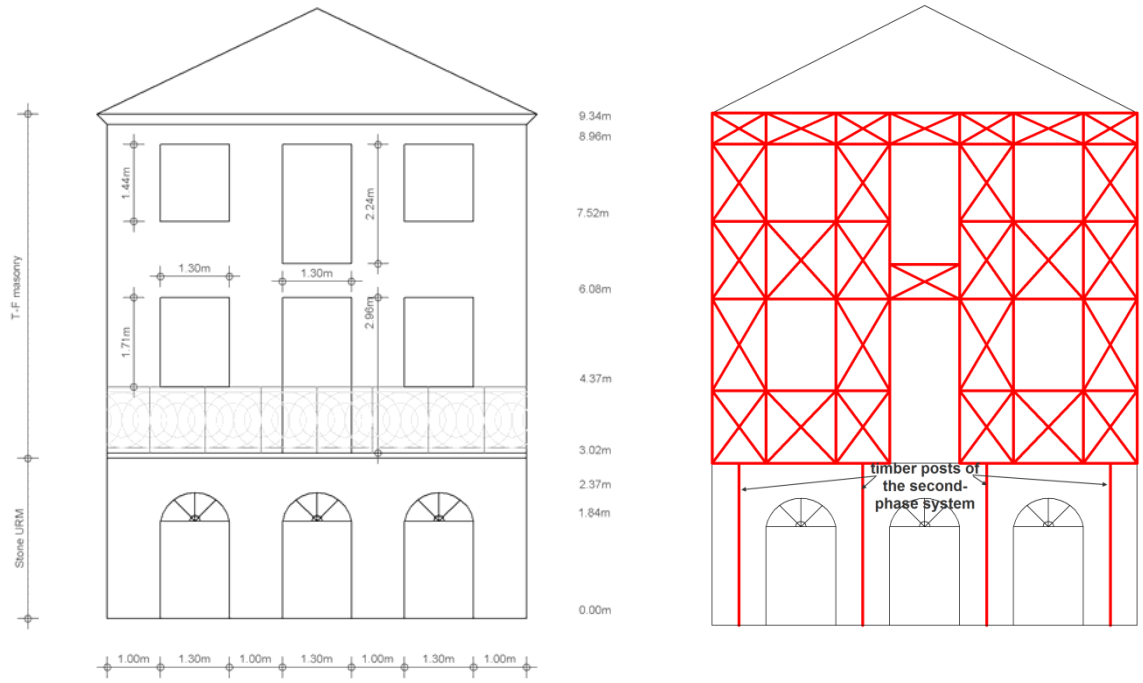

Figure 5. Berykiou building in the central square of Lefkas city: (a) façade geometry and (b) timber elements of TFM walls and the ground storey second-phase system in red.

A typical section of timber elements of timber-framed masonry is assumed (10×10 cm) and the thickness of TFM infills is also assumed as 10 cm. Timber posts of the secondary system have a section 15×15 cm. The L and T-shaped angles between the beams and posts (**Figure 2**) together with the carpentry joints and the masonry infills result in a moment resisting connection of the timber frame. Thus, the connections of beams and posts are considered stiff in contrast with the connections of the diagonals which are set as 'free'.

The secondary system of the timber column in the ground storey (**Figure 5**b) has a substantial displacement capacity due to the ductility of timber. The activation of the secondary system upon the exceedance of the displacement capacity of the unreinforced masonry ground storey piers will add a displacement reserve which allows the structure to withstand the induced energy from the seismic excitation. Referring to **Figure 3** two bounding cases are considered for column end restraints, i.e. fully clamped or free to rotate**.**

Mechanical properties of wood correspond to timber class C24 and service class II according to EC-5 (CEN 2004a) (see **Table 1**). Experiments (Hendry 1998) on traditional stone masonry specimens made of two outer wythes of ashlar stones and an inner core of rubble have shown that these walls present relatively low strength compared to that of the stones per se. In this regard a conservative value of the compressive strength is adopted (Table 1). Furthermore, a simplified beam model is utilised, which takes into account the possible crack mechanisms of a pier submitted to bending with vertical load: (i) rocking, (ii) sliding shear and (iii) diagonal shear cracking (Kappos et al. 2002; Penelis 2006). Masonry is considered isotropic in this beam-modelling approach as the strength differences in the two axes are not substantial (Naraine and Sinha 1991).

Table 1. Mechanical properties for the materials used in the model in the longitudinal (x) and the transversal (y) direction.

	Masonry	Wood
Compressive strength $f_{c,x}$ [MPa]	3.50	18.9
Compressive strength $f_{c,y}$ [MPa]	3.50	4.77
Tensile strength $f_{t,x}$ [MPa]	0	18.9
Tensile strength $f_{t,y}$ [MPa]	0	4.77
Modulus of elasticity E_x [MPa]	1750	11000
Modulus of elasticity E_y [MPa]	1750	370
Shear modulus G [MPa]	673	690
Weight [kN/m^3]	20	3.5
Poisson ratio v	0.2	0.3

2.3 Analysis and pushover curves of the typical building

A 2D plane model of the façade is set up in SAP2000. A macro-model technique is adopted (Kouris and Kappos 2014) based on lumped plasticity point hinges in the strut elements. This model has been based on the micro plasticity model of Kouris and Kappos (2012). However, the computational effort to derive reliable results for entire buildings is the major drawback of the micro-model that limits its applicability. On the other hand macro-models should be applied only in cases of usual geometry. If this is not the case a hybrid model should be used based on the sub-structuring technique to allow for complex configurations (Kouris et al. 2014). Application of both procedures to certain cases with usual geometry has shown negligible differences among them (Kouris 2012).

The building model comprises strut elements and non-linear axial hinges on the diagonals to accommodate all plastic deformation of the timber-framed walls. The methodology requires discretization of the real timber-framed structure in individual TF panels. A set of empirical formulas are used to determine the NL law of the axial hinges (Kouris 2012), and then they are inserted in the diagonals as point plastic hinges on the global model.

The micro-model is based on a Hill-type plasticity model which efficiently describes the orthotropic behaviour of timber. The yield and failure surfaces are presented in Figure 6. Details about the micro-model can be found in Kouris and Kappos (2012).

TF walls are modelled by axial force-axial deformation (N-ε) nonlinear lumped plasticity hinges in the diagonals (Kouris 2012). Modification of the axial stiffness of the diagonals is required to take into account their sliding (Kouris et al. 2014):

$$k_s = \frac{\left(H^2 + L^2\right)^{3/2} + H^3}{EA} \cdot \frac{1}{L^2} \cdot \frac{V_y}{\delta_y} \tag{1}$$

In Equation (1) E is the Young's modulus of timber, A is the area of the section, δ_y and V_y are the corresponding displacement and shear force at yielding and L, H the panel dimensions. The connections between timber beams and timber columns are set as pinned.

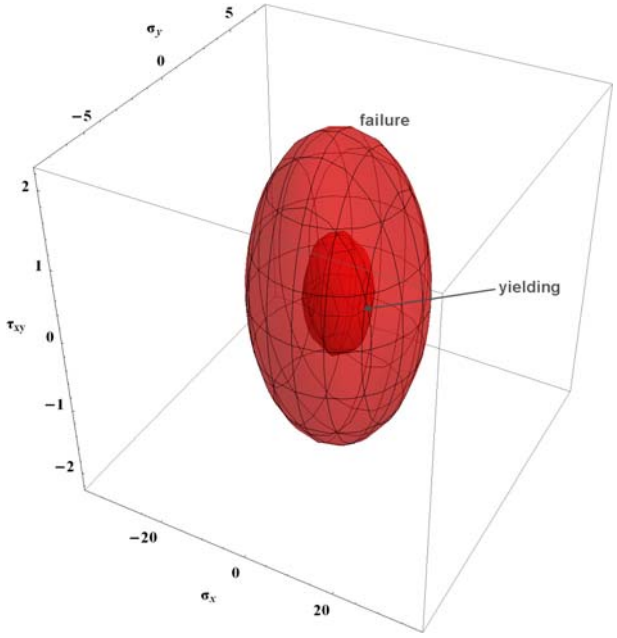

Figure 6. The yield and failure domains of Hill yield criterion in the 3D space.

The methodology follows nine steps described in detail in Kouris (2012) and summarised below:

1. Discretization of the building into individual TFM panels.
2. The tributary vertical load is calculated for each TFM panel.
3. The empirical formulas (Kouris 2013) are applied to define the constitutive law of each panel in terms of horizontal shear vs. displacement.
4. The elastic stiffness of the panel is corrected using Equation 1.
5. The NL law of the plastic hinges in the diagonal struts is defined in terms of axial load vs. deformation.

The unreinforced masonry piers of the ground storey are modelled using moment-rotation (M-θ) lumped plasticity hinges according to (Kappos et al. 2002; Penelis 2006). This model requires the estimation of the axial load of the piers from a preliminary elastic analysis. Then, two parallel analyses are carried out to determine the M-θ relationship of each critical section of the piers; one for flexural failure and a second for shear failure. For the former a fibre section analysis procedure is followed where in each step the curvature φ is defined from the compression strain of the masonry pier ε and the length of the compression zone χ:

The shear force vs. shear deformation relationship is obtained from experimental data (see Penelis 2006). Then, these two analyses are combined to give the constitutive M-θ law of the critical sections (top and bottom) of each pier. The ultimate deformation of the section is controlled either from shear or from bending; here failure of the piers appears to occur due to rocking response due to the relatively low vertical load from the upper storeys. An example of the M-θ constitutive law is presented in **Figure 7**. The modulus of elasticity for masonry is taken as $500f_{cw}$ where f_{cw} is the compression strength of masonry (FEMA 2000; Kappos et al. 2002), which was found compatible with the elastic modulus defined from section analysis:

$$E_m = \frac{M_y}{\varphi_y I} \tag{2}$$

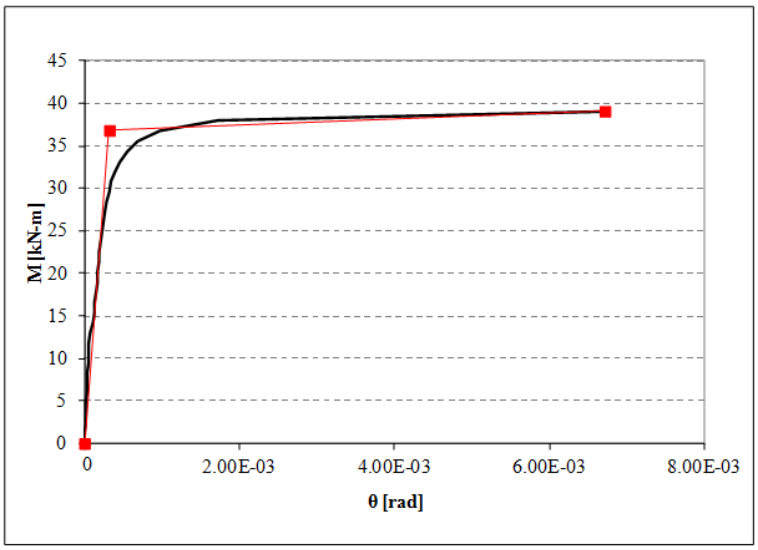

Figure 7. The M-θ constitutive law of the first pier from the left on the bottom edge (see Fig. 5).

The key feature of the dual system is the activation of the timber-posts of the ductile secondary system after the failure of the ground floor URM piers. During the first phase of the seismic response (primary system) the contribution of the timber posts to the lateral capacity is unimportant. Moreover, their contribution to the vertical load at this phase is questionable given that shrinkage phenomena have taken place in the wood. In this regard, the two systems are considered here sequentially.

Elastic dynamic analysis of the structure assuming nodes fixed on the ground is performed and a natural period equal to $T_{1,1}$=0.19 s is found for the structure (second subscript refers to system 1, prior to failure of ground storey masonry). The first mode activates 92% of the total mass. The first mode shape is close to a triangular one (**Figure 8**a). Compared to elastic analysis by Vintzileou et al. (2007) for a similar, but two storey, building the first natural period is longer. This is attributed to the inclusion of the masonry infills in their model and the difference in the total height.

This elastic model with natural period equal to 0.19 s has two diagonals active in each panel; however, this linear elastic response is very short and for a broader displacement range of the response only the diagonal in compression will be active (Kouris and Kappos 2012). For a linear model with elastic modulus E and two diagonals with section area A and lengths in compression L_c and in tension L_t, respectively, the equivalent modulus of elasticity E' for the frame with only compression diagonals can be found as follows:

$$\frac{E'A}{L_c} = \frac{1}{2}\left(\frac{EA}{L_c} + \frac{EA}{L_t}\right) \tag{3}$$

Applying Equation 3 to the linear elastic model, the new natural period of the quasi-elastic structure is found to be 0.23 s. This quasi-elastic structure, which is representative of the response for the best part, is valid as long as the piers do not fail. At that point the secondary system will be activated; it is pointed out that although the two models in **Figure 8** look the

same, the ground storey elements are very different in each case (initially masonry walls, then timber frame).

Unlike the primary system, the secondary system has a first mode of vibration which is almost uniform (**Figure 8**b). The first natural period of the second-phase system is $T_{1,2}$=1.39 s (much longer than that of the initial system) and the mass activated exceeds 90% of total. It is noted that the mass of the system is now significantly lower as the mass of the damaged piers is not deemed to form part of the vibrating structure. In this regard the initial mass was equal to 35.20 kN-s^2/m (ton) whereas the mass of the second-phase system without the masonry piers is now 27.47 kN-s^2/m.

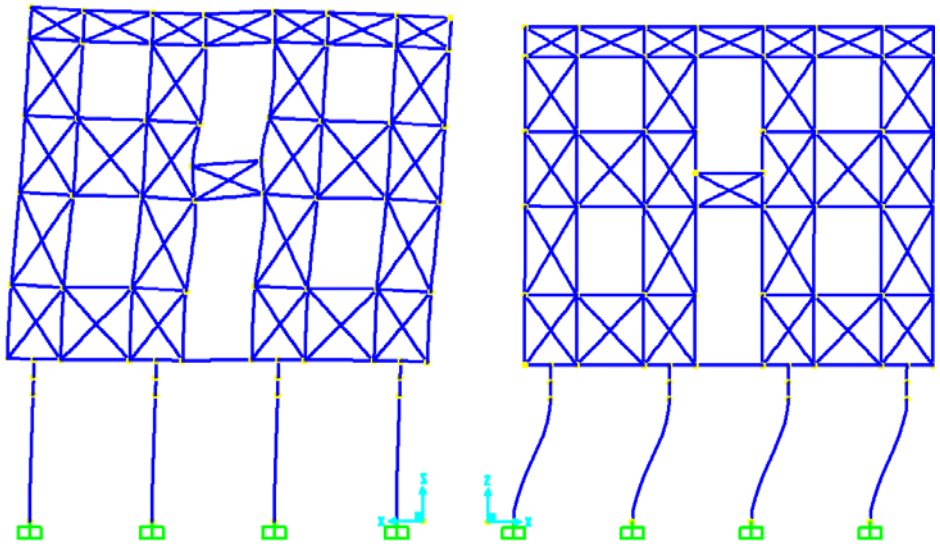

Figure 8. The first natural mode of vibration of the Berykiou building for: (a) initial system and (b) second-phase system.

These two co-existing systems perform in a rather diverse way. The primary system is close to what the codes (FEMA 2000; CEN 2004b) specify as triangular distribution of modal displacements along the height of the structure. On the other hand the second-phase system resembles the uniform distribution when the storey mechanism forms (similar to the familiar pilotis type of behaviour). The two systems are modelled separately for two reasons:

(i) the considerable differences in modal characteristics of these two systems result in different shape of the pushover curve, and

(ii) introducing a softening branch in the curve is prone to numerical instabilities that can cause errors and/or early termination of the analysis.

Hence, two different pushover load patterns are applied to each system corresponding to the respective first mode loads; the initial system is loaded with a triangular load pattern, whereas the second-phase system is loaded with a uniform pattern. The failure mechanism of the primary system at the end of its NL static analysis is depicted in **Figure 9** where plastic hinges are indicated by a different colour associated to their damage state. 'Collapse' of the building is due to the development of a ground storey mechanism. However, the upper TFM storeys have suffered considerable damage as manifested by the widespread inelastic deformations of the TFM panels. Indeed, development of hinges in the ground storey is

preceded by the occurrence of the TFM wall hinges. However, the evolution of the plastic deformation in the ground storey is rather quick and finally dominates the failure mechanism. Capacity curves from the non-linear static analyses of the two system in terms of base shear V vs. top displacement Δ are presented in **Figure 10**a. The bilinearisation of the pushover curve (dashed line) follows the equal energy rule, i.e. equating the areas below and above the bilinear curve and the actual pushover curve (Panagopoulos and Kappos 2009).

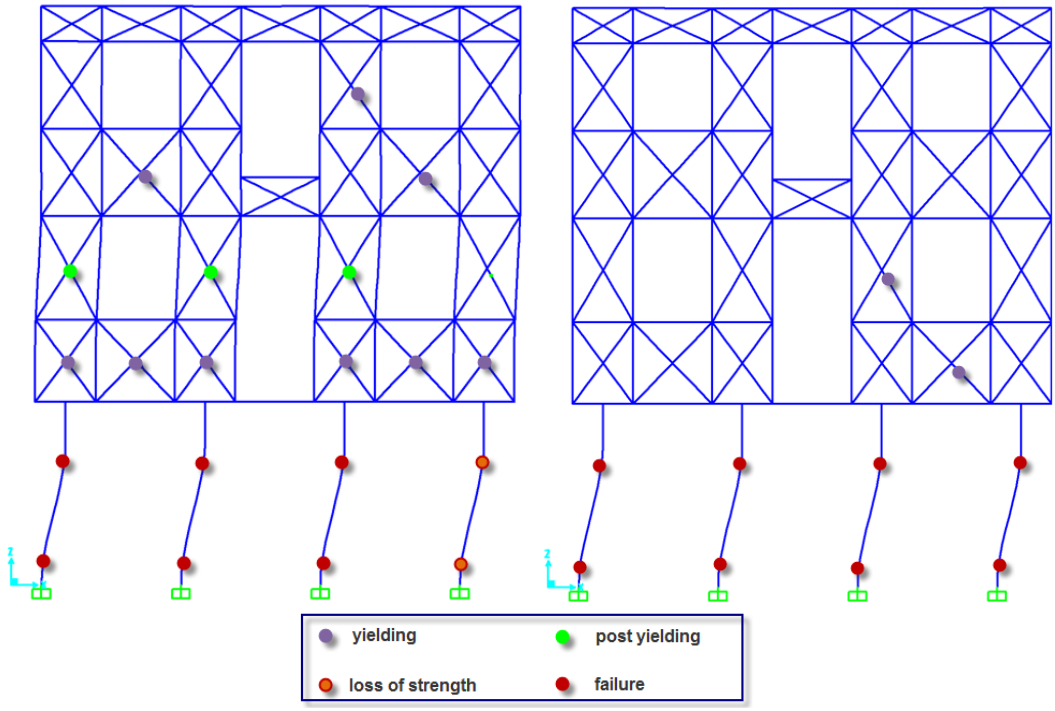

Figure 9. Failure mechanism of the initial (left) and the second-phase (right) system of 'Berykiou' building.

On the other hand, NL static analysis of the second-phase system predicts collapse of the timber posts of the ground storey and negligible inelastic deformation in the upper storeys; the latter remain almost intact and the entire plastic deformation is concentrated in the ground storey which is a typical performance of a structure with a storey side-sway mechanism.

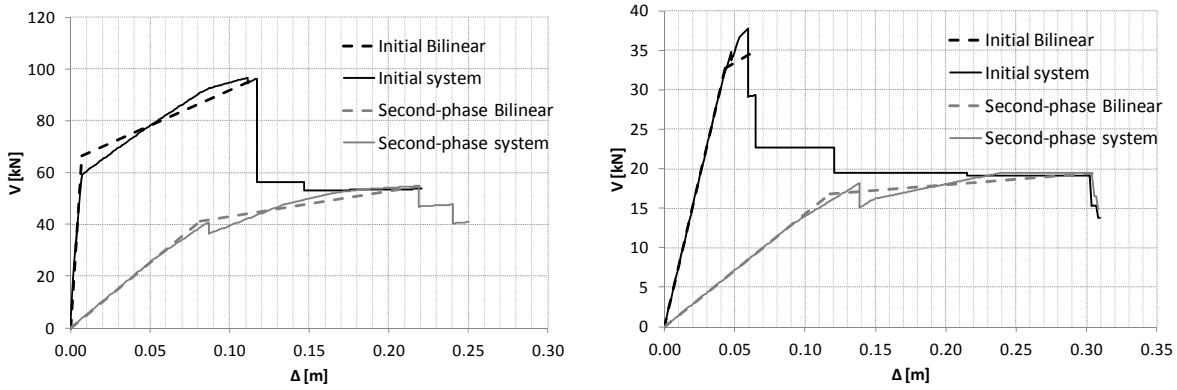

Figure 10. Pushover curves of the initial and the second-phase system of the 'Berykiou' timber-framed masonry building with: (a) full restraints and (b) flexible supports (SSI).

These two mechanisms in the real building coexist and interact; activation of the secondary system occurs after failure of the unreinforced masonry ground storey piers but until then it follows the deformation of the primary system. Consequently, the initial soft branch of the secondary system (grey line in **Figure 10**a) does not appear in reality and combination of the two pushover curves is in order; failure of the ground storey piers constitutes the point wherein the two curves should be joined. Then, the resulting curve is idealised as a multi-linear one (points A to E) that allows definition of a yield point. The following segments are depicted: (i) the quasi-elastic part (A-B) where –in principle- no plastic deformation appears, (ii) the second part (B-C) where non-linear deformation occurs in both the ground storey and the timber-framed masonry upper storeys, (iii) the sudden drop in the base shear capacity during the third part of the capacity curve (C-D) due to the collapse of the ground storey unreinforced masonry piers, and (iv) the residual capacity during the fourth part of the response (D-E) wherein the building has a reserve displacement capacity under an almost constant base shear. The relatively low axial force on the unreinforced masonry piers resulting from the overturning moment leads to almost simultaneous failure of the ground storey unreinforced masonry piers.

2.4 Variations of the typical building

2.4.1 Soil-Structure Interaction

Previous analyses have been carried out without considering any interaction between the building and the soil as full fixity has been assumed at the basis of the piers. However, the city of Lefkas is situated on soft alluvial deposits (Karakostas et al. 2005), which give rise to compliance of the unreinforced masonry foundations. The latter are usually strengthened with a substructure made of layers of logs, to increase their stiffness (Makarios and Demosthenous 2006; Porphyrios 1971). Dynamic impedances for this kind of foundation and this type of soil have been estimated as k_{sdv}=2400 kN/m^3 for the vertical direction and k_{sdh}=1600 kN/m^3 for the

horizontal one to account for soil – structure interaction (SSI) (Karakostas et al. 2005; Makarios and Demosthenous 2006). The building foundation of the unreinforced masonry pier of the ground storey has the dimensions shown in **Figure 11**. In this case where SSI is taken into account the restraints of the piers are assumed pinned at their ends in line with the detailing shown in **Figure 3**c (Porphyrios 1971; Vintzileou et al. 2007). The natural period of the initial system with SSI is $T_{1,1,SSI}$ = 0.7 s and the activated mass is now lower (78%). The second mode is a rigid body motion and activates almost the remaining part of the mass (21%).

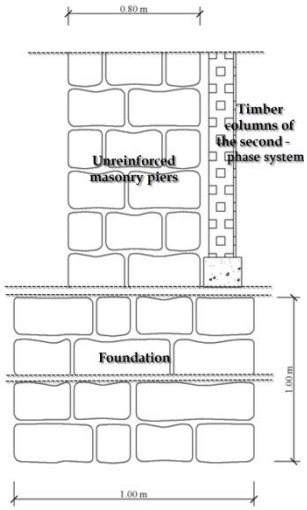

Figure 11. Configuration of the unreinforced masonry piers foundation.

The capacity curves of the two-storey building modelled with SSI are given in **Figure 10**b. The main differences with the fixed end model are with respect to the following two points; (i) the second part of the capacity curve B-C is very limited since the moments that are developed at the top end of the masonry piers for the same base shear V are twice as high (225%) due to the pinned bottom end; (ii) for the same reason the total base shear V that the building can carry is halved in value.

2.4.2 One and two storey buildings

The timber-framed masonry building stock in Lefkas includes also two-storey edifices usually for commercial use (stores) and single-storey structures housing the 'lower class' families (Porphyrios 1971). The former type of TFM structures takes advantage of the dual system (§ 2.1) whilst the single-storey houses are made of pure timber-framed masonry without the second line of reserve capacity i.e. the secondary system.

The geometry of the two-storey typical building is similar to the three-storey building apart from the total height which is increased up to 6.7 m (**Figure 12**a). The model is presented in **Figure 12**a where the ground storey columns represent the masonry piers and the diagonally braced timber frame of the first storey the timber-framed masonry. Materials, loads and member sections are the same as in the three-storey building (see **Table 1** and §2.2

respectively). Two different foundations are considered: (i) fixed end foundation (**Figure 12**a), and (ii) pinned-ended foundation with SSI (modelled as previously described).

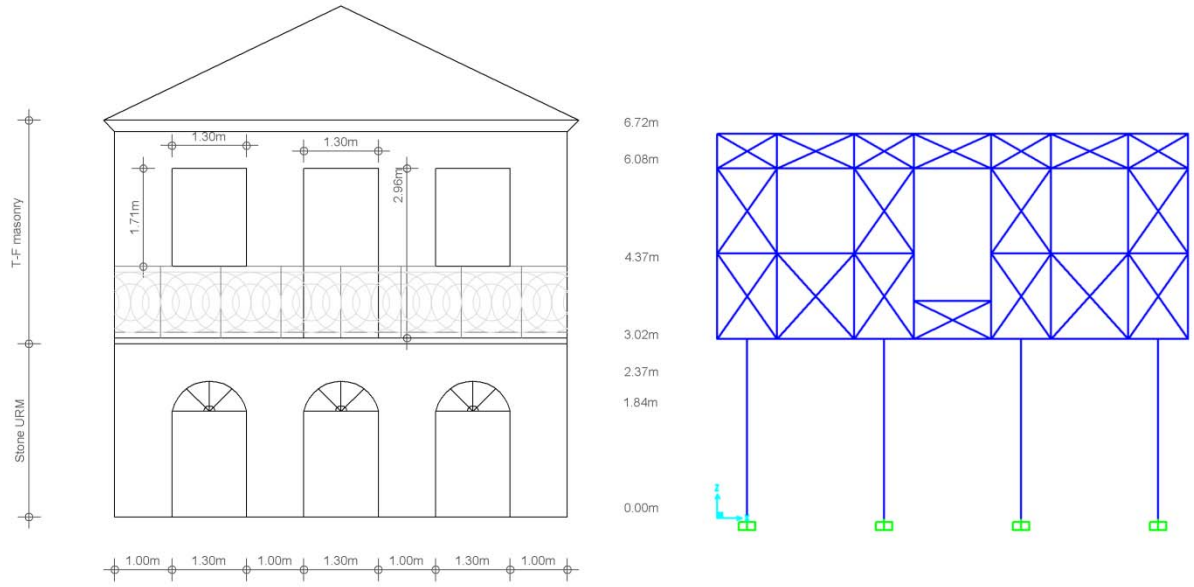

(a)

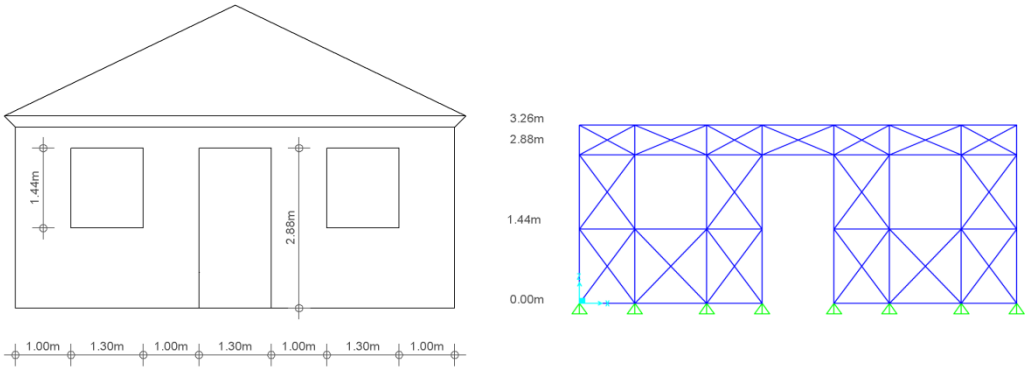

(b)

Figure 12. Modelling of (a) two-storey building with dual system and (b) single-storey building with pure TFM system.

The geometry of the single-storey building presented in **Figure 12**b follows also similar layout and the total height reaches up to 3.3 m. The timber-framed panels have length 1 m with openings measuring 1.30 m×1.44 m. Materials, loads and member sections are the same as in the three-storey building. The model presented in §2.3 for timber-framed masonry is used, shown in **Figure 12**b. Two cases of foundation restraints are also considered i.e. with and without SSI.

Pushover curves for the two-storey building with the dual system and the single-storey building with the pure TFM system are given in **Figure 13**a and b, respectively. The single storey building presents, as expected, a rather bilinear response.

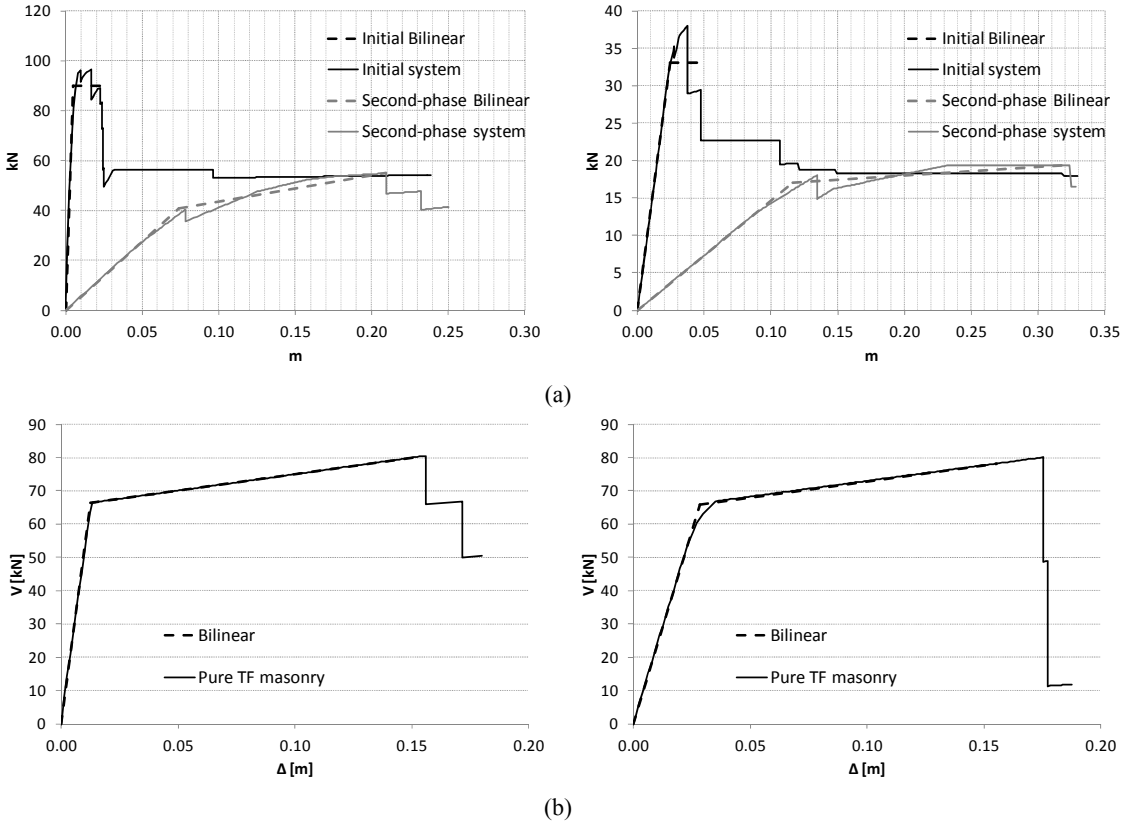

Figure 13. Pushover curves derived for full fixity on the left and flexible supports (SSI) on the right: (a) two-storey timber-framed masonry building with dual system, and (b) single-storey building with pure timber-framed masonry system.

Table 2 summarises the cases of analysed buildings. Each building is allocated a three-prefix designation (columns 2, 3, and 4 of the table) which is used in the remainder of the chapter.

Table 2. List of analysed buildings and pertinent notation.

Building Case	Building Designation		
	1st term	2nd term	3rd term
Three storey building - primary system with fixed foundation	3st	fix	pr
Three storey building - primary system with SSI	3st	ssi	pr
Three storey building - secondary system with fixed foundation	3st	fix	sc
Three storey building - secondary system with SSI	3st	ssi	sc
Two storey building - primary system with fixed foundation	2st	fix	pr
Two storey building - primary system with SSI	2st	ssi	pr
Two storey building - secondary system with fixed foundation	2st	fix	sc
Two storey building - secondary system with SSI	2st	ssi	sc

Single storey building (pure timber-framed) with fixed foundation	1st	fix	-
Single storey building (pure timber-framed) with SSI	1st	ssi	-

3. CAPACITY AND FRAGILITY CURVES

3.1 Capacity curves

Fragility curves are derived based on the key assumption that the structure under consideration possesses the mean characteristics (geometrical, material etc.) leading to a seismic performance that can be assumed as the average of that typology of buildings (Kircher et al. 2006). The studied (§2) timber-framed masonry building is selected as representative of the typical timber-framed masonry building in Lefkas. Consequently, the seismic behaviour of this class of buildings can be expressed in terms of their 'average' pushover curve. The capacity spectrum method (Freeman 1998) based on inelastic demand spectra (Fajfar 1999) is used here to relate pushover curves with seismic demand. Thus, pushover curves are transformed into capacity curves, i.e. the pushover curve of the corresponding equivalent SDOF (single degree of freedom) system. This transformation is implemented using properties of the predominant mode in the considered direction. The validity of this procedure depends on the contribution of the first mode, which in this case is over 90%, which ensures reliable results. The procedure follows two steps: (i) the effective mass m^* and the modal participation coefficient Γ_1 of the first mode are estimated using the following Equation 4 and then, (ii) the spectral acceleration S_a and the spectral displacement S_d are estimated from Equation 5 based on the effective mass m^* and the modal participation coefficient Γ_1.

$$m_1^* = \frac{[\varphi_1^{\mathrm{T}} m]^2}{\varphi_1^{\mathrm{T}} m \varphi_1}$$
$$\Gamma_1 = \frac{\varphi_1^{\mathrm{T}} m}{\varphi_1^{\mathrm{T}} m \varphi_1} \quad (4)$$

$$S_a = \frac{V}{m_1^*}$$
$$S_d = \frac{u_{1,roof}}{\Gamma_1 \varphi_1} \quad (5)$$

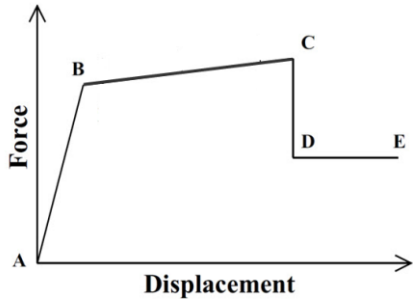

Figure 14. The five points defining the simplified pushover curves.

It is noted that the effective mass m^* and the modal participation coefficient Γ_1 are different for the primary and the secondary system of the same structure due to different mass and mode shape of each system.

A capacity curve is usually defined by two points; (i) the yield point B that represents the transition from elastic to inelastic deformations, and (ii) the (ultimate) capacity point C which represents failure of the piers of the primary system. Nevertheless, for the Lefkas dual system buildings two additional points have to be defined: (iii) point D related to the yielding of the second-phase system and (iv) point E representing collapse of the secondary system of the ground storey, and eventually of the entire building. This sequence of points shown in **Figure 14** specifies the main four representative stages of the seismic performance of timber-framed masonry buildings with a dual system.

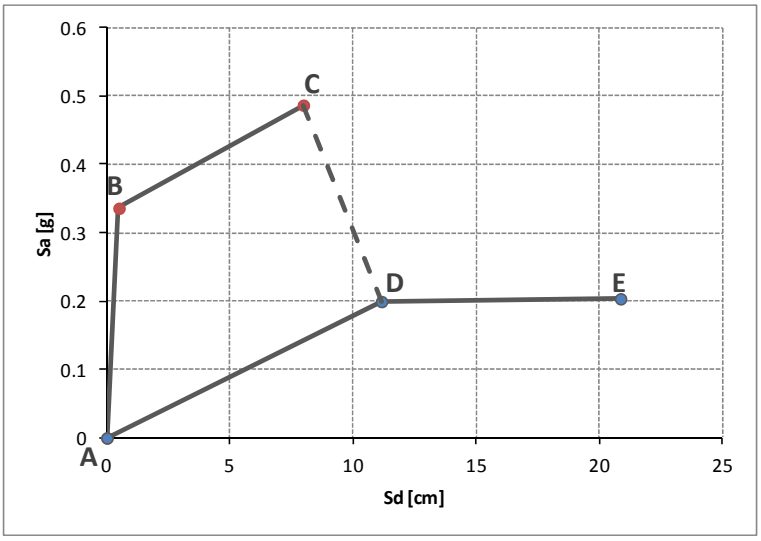

Figure 15. The capacity curve for the 3st_fix building (see also Table 2).

An example of this capacity curve is shown in **Figure 15** for the three storey timber-framed masonry building with fixed foundations. The capacity curve results from the combination of the respective curve of the initial and the second-phase systems. Values for the entire set of buildings are given in **Table 3** (the designation is described in Table 2).

Table 3. Spectral displacements [in cm] and spectral accelerations [in g values] for the capacity curves.

		B	C	D	E
3st_fix_pr	S_d	0.49	7.98		
	S_a	0.34	0.49		
3st_fix_sc	S_d			11.16	20.87
	S_a			0.20	0.20
3st_ssi_pr	S_d	2.89	4.34		
	S_a	0.11	0.12		
3st_ssi_sc	S_d			6.40	29.99
	S_a			0.07	0.07
2st_fix_pr	S_d	0.32	1.60		
	S_a	0.37	0.37		
2st_fix_sc	S_d			2.39	20.63
	S_a			0.26	0.27
2st_ssi_pr	S_d	1.79	3.47		
	S_a	0.12	0.12		
2st_ssi_sc	S_d			3.65	24.99
	S_a			0.10	0.10
1st_fix	S_d	1.27	15.09	-	-
	S_a	0.62	0.75	-	-
1st_ssi	S_d	2.83	15.53	-	-
	S_a	0.62	0.73	-	-

3.2 Fragility curves

3.2.1 Fragility curves in terms of spectral displacement

It is well documented in the literature that fragility curves can be described by (cumulative) normal, lognormal, or beta distributions (Whitman et al. 1997; Vamvatsikos et al. 2010b). The lognormal distribution is adopted here since it describes adequately the evolution of damage (Kircher et al. 2006). This distribution is expressed by the equation:

$$\mathrm{P}\left[ds \geq ds_i \middle| A_g\right] = \Phi\left[\frac{1}{\beta_{ds,i}} \ln\left(\frac{A_g}{\overline{A}_{g,dsi}}\right)\right] \tag{6}$$

In Equation 6 Φ is the cumulative distribution function of the lognormal distribution, $\beta_{ds,i}$ is the standard deviation of the natural logarithm of the damage state i and $\overline{A}_{g,dsi}$ the mean value of the appropriate measure that represents seismic intensity (here spectral displacement $\overline{S}_{d,i}$) at which the building reaches the threshold of damage state i.

Standard deviation $\beta_{ds,i}$ of the lognormal value of $\overline{A}_{g,dsi}$ defining damage state ds represents a series of uncertainties for each fragility curve and in general is not the same for every damage state. The variability included in $\beta_{ds,i}$ can be summarised in three contributors (Kappos et al. 2006; Kircher et al. 2006): (i) uncertainty due to the ground motion β_D, (ii) uncertainty in the response of the structure (capacity curve), and (iii) uncertainty in the definition of damage states. A reasonable and convenient assumption is to consider that these

three sources of variability are statistically independent and thus, the total standard deviation $\beta_{ds,i}$ is estimated as the square root of the sum of the squares of each term.

An alternative procedure to estimate the total standard deviation $\beta_{ds,i}$ is by making recourse to the binomial distribution instead of the lognormal one (Barbat et al. 2008; Lagomarsino 2006). The binomial distribution involves only one parameter, the mean value of the spectral displacement $\overline{S}_{d,i}$:

$$P_i = \frac{n!}{i!\cdot(n-i)!}\cdot\left(\overline{S_{d,i}}\right)^i\cdot(1-\overline{S_{d,i}})^{n-i}\;|_{i=1-n} \tag{7}$$

Then the correlation of the two distributions (Equations 6 and 7) to derive the total standard deviation $\beta_{ds,i}$ of each damage state is based on the 50% probability of the lognormal distribution corresponding to the spectral displacement threshold of each damage state $\overline{S}_{d,i}$.

Regarding the damage states, several definitions have been proposed for each building class (Hill and Rossetto 2008). The number of different damage states may vary from 3 to 6, excluding the zero damage state (DS0). Eurocode 8-3 (CEN 2005) provides the definition of only three damage states: near collapse, significant damage and damage limitation for a structure that has undergone economically repairable cracking; these definitions appear to be tailored to structures with a single lateral load resisting system, such as reinforced concrete frames (with or without masonry infills) or masonry buildings without timber framing. Four damage states have been considered here, ranging from DS1 (negligible to small damage) to DS4 (total collapse); their designation is provided in **Table 4**. Each damage state is related to a certain degree of loss, usually defined in terms of structural performance or of cost of repair (monetary index) (Kappos et al. 2006). In the latter case loss may reach values over 100% due to an excessive repair cost with respect to the cost of replacement.

For the timber-framed masonry buildings the following remarks are in order:

- The yield point B (**Figure 14**), which is the intersection of the initial elastic branch with the second branch should normally be the instant where the first element (masonry pier) of the structure 'yields' (in the context of a bilinearised resistance curve). For the case of **Figure 9** this element would be the left masonry pier in the ground storey. However, when the actual resistance ('pushover') curve is bilinearised on the basis of equal energy then this point B is an equivalent yield point which no more reflects the instant of the first yield but rather some (limited) nonlinear response is generally expected prior to reaching this point. In this regard this damage state is deemed as slightly below the 'damage limitation' limit state of Eurocode 8 (CEN 2004b).
- Point C refers to the initiation of heavy damage with the failure of ground storey masonry piers. From point B to point C of the response, piers gradually suffer damage (nonlinear response) and so does a number of timber frames of the upper structure. From this set of analyses (**Table 2**) it is found that at 40 to 60% of the distance between B and C all base piers experience a certain level of nonlinear response. Thus, this instant can be taken as the threshold of moderate damage in the building.
- Point D refers to the displacement where all the base masonry piers have failed and the secondary system is activated. Masonry piers are generally repairable but permanent deformation (drift) may drive the repair cost over the cost of replacement (Vintzileou et al. 2007). This damage state would correspond to the qualitative

description of the ‘significant damage’ limit state of Eurocode 8 (CEN 2004b) as regards the damage to the structural and non-structural members, permanent drifts and potentiality of restoring damage. From the strength point of view, the structure is close to Eurocode ‘near collapse’ LS as the lateral load capacity has been substantially reduced, however, due to the dual nature of the TFM system this is a stable system that can withstand significant further displacement, unlike e.g. concrete frames that have lost a large fraction of the strength.

- Point E refers to the maximum displacement capacity of the structure. At this point the building is unable to absorb more seismic energy and essentially collapses. Consequently, this signifies the collapse of the structure. This ultimate state coincides with the ‘near collapse’ limit state of Eurocode 8 (CEN 2004b).

Table 4. Definition of damage states.

Damage State	Designation
DS0	No damage
DS1	Negligible to small
DS2	Moderate
DS3	Substantial to heavy
DS4	Very heavy (partial or total collapse)

Mean spectral displacements $\overline{S}_{d,i}$ are computed according to the previous discussion of the damage stages through the following expressions:

$$\overline{S}_{d1} = \delta_y = \delta_B \tag{8a}$$

$$\overline{S}_{d2} = 0.4 \times (1.5\delta_y + \delta_C) \tag{8b}$$

$$\overline{S}_{d3} = \delta_C \tag{8c}$$

$$\overline{S}_{d4} = \delta_u = \delta_E \tag{8d}$$

In Equations 10 δ_i are the displacements of points i (i.e. points A to D according to **Table 3**). The points calculated from Equations 8 for the three-storey TFM building with fixed foundations are shown in **Figure 16**.

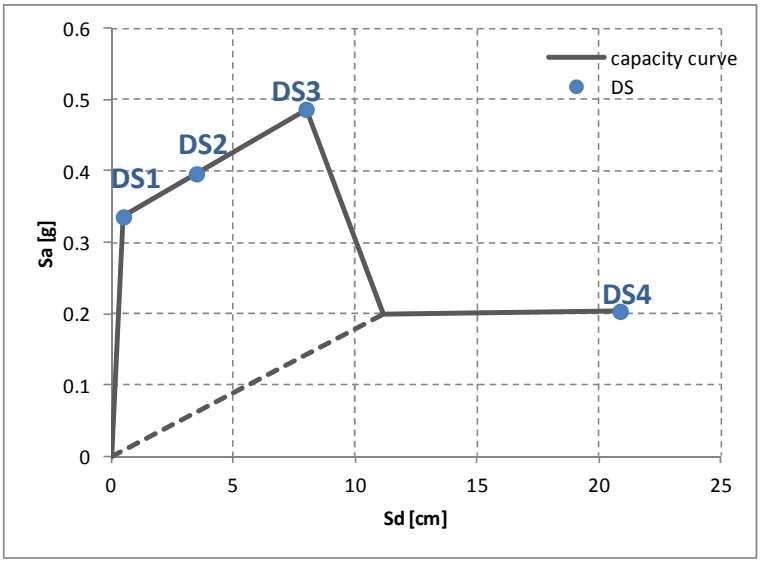

Figure 16. The thresholds of the damage states for the 3st_fix building.

Applying Equations 8 with the values of **Table 3** and the aforementioned methodology for standard deviation $\beta_{ds,i}$ the fragility curves (probability of exceedance vs. spectral displacement S_d) for the timber-framed masonry buildings with dual system were generated. It is worth noting here that defining fragility curves in terms of S_d, has the major advantage of making them independent of the ground motion characteristics, unlike those in terms of PGA that have to be adjusted to the representative response spectrum of the region wherein they are used (Kappos et al. 2010). However, it also has the disadvantage that it makes much harder their calibration against actual damage data, since very few such data are available in terms of displacement.

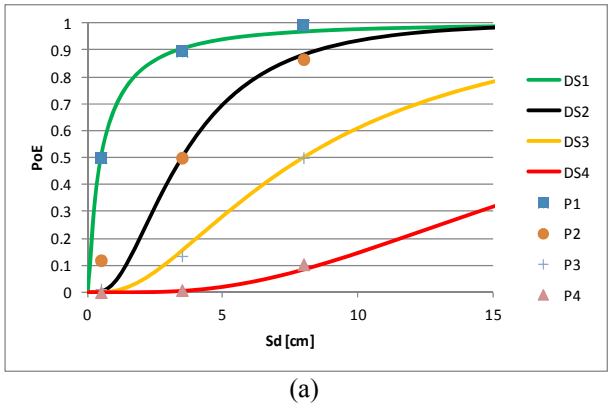

(a)

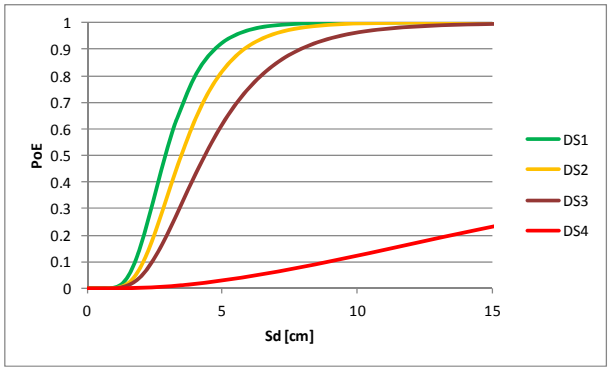

(b)

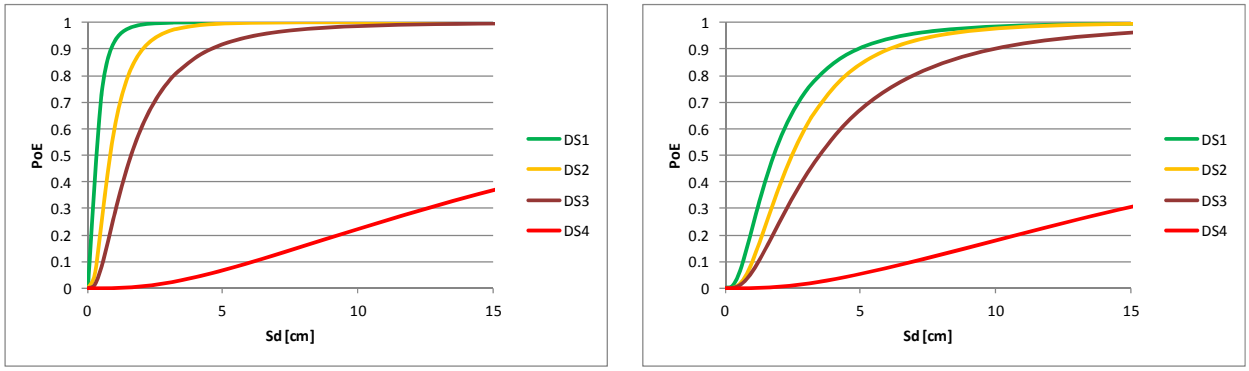

(c) (d)

Figure 17. Fragility curves for the following building typologies (Table 2): (a) 3st_fix, (b) 3st_ssi, (c) 2st_fix and (d) 2st_ssi.

Figure 17 shows the fragility curves for three and two storey TFM buildings with a dual system. The least-square minimisation of the error (i.e. the difference squared) between the binomial (points $P1_i$, $P2_i$, $P3_i$ and $P4_i$ for each DS_i) and the lognormal distributions is presented in **Figure 17**a. Hence, the standard deviation β_i of this procedure is purely a mathematical outcome rather than a value extracted from structural analyses. It is seen that DS1 (light damage) will be reached for rather low earthquake intensity (expressed herein in terms of displacement). Taking into account the deformability of the ground, DS1 shifts to substantially higher displacements, which might mean higher intensities (**Figure 17**b and d); however, the displacement demand increases with the period and, as seen in §2, the period of the buildings on soft soil is longer than that fixed to the ground, and also depends on the type of response spectrum used for estimating demand. A similar trend is noted with respect to DS4, whose probability of exceedance decreases for the same values of spectral displacement. On the contrary, intermediate damage states (DS2 and DS3) shift towards lower displacements (increase in fragility).

Damage states for the single-storey pure timber-framed masonry buildings do not follow the previous definition (Equations 8) as their capacity curves are described by only two points (**Table 4**), point B that is the yield point and point C that is the collapse point. A reasonable definition of the damage states is in line with the similar category of unreinforced masonry buildings (Barbat et al. 2008; Kappos et al. 2006; Pujades et al. 2010):

$$\overline{S}_{d1} = 0.7\delta_y \tag{9a}$$

$$\overline{S}_{d2} = \delta_y = \delta_B \tag{9b}$$

$$\overline{S}_{d3} = \delta_y + \left(\delta_u - \delta_y\right)/4 \tag{9c}$$

$$\overline{S}_{d4} = \delta_u = \delta_C \tag{9d}$$

In Equations 9 δ_y is the yield displacement and δ_u is the ultimate displacement (i.e. points B to C respectively according to **Table 3**). Equations 9 are conservative for the first two damage states (DS1 and DS2). A similar alternative definition is the following:

$$\bar{S}_{d1} = 0.9\delta_y \quad (10a)$$

$$\bar{S}_{d2} = 1.2\delta_y \quad (10b)$$

$$\bar{S}_{d3} = \delta_y + \left(\delta_u - \delta_y\right)/4 \quad (10c)$$

$$\bar{S}_{d4} = \delta_u = \delta_C \quad (10d)$$

The previous definitions (Equations 9 and 10) for the single-storey pure timber-framed masonry building with fixed foundations are compared in **Figure 18**.

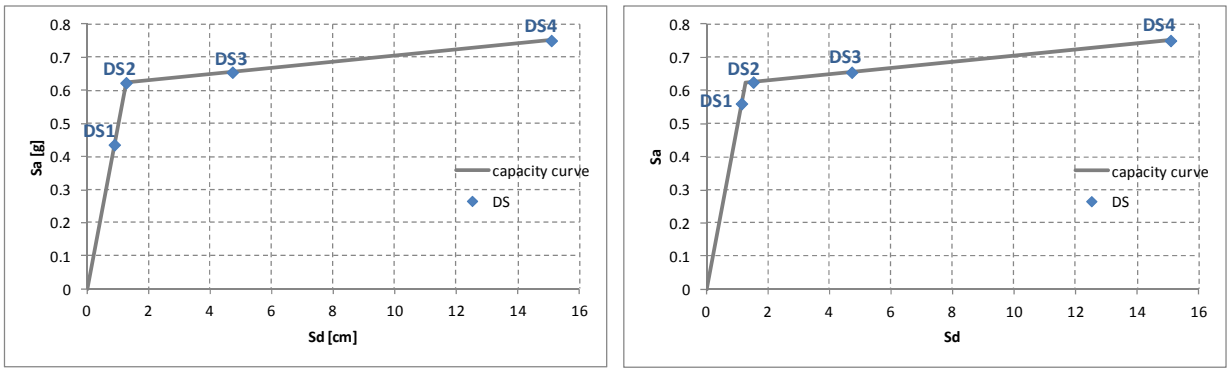

(a) (b)

Figure 18. Various definitions of damage states on the capacity curve of 1st_fix buildings: (a) Equations 9 and (b) Equations 10.

Application of Equations 9 and 10 with the values of **Table 3** for the yield and ultimate spectral displacement results in the fragility curves (probability of exceedance vs. spectral displacement S_d) for the single storey pure timber-framed masonry buildings shown in **Figure 19.**

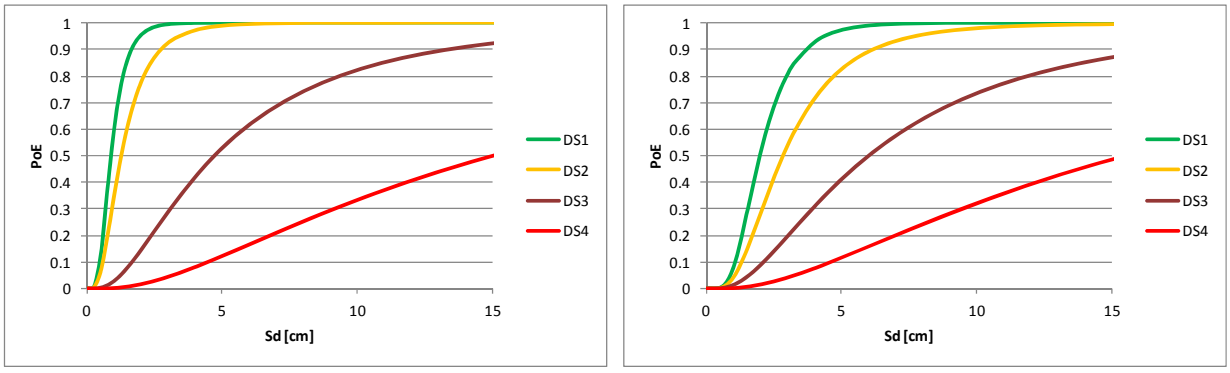

(a) **(b)**

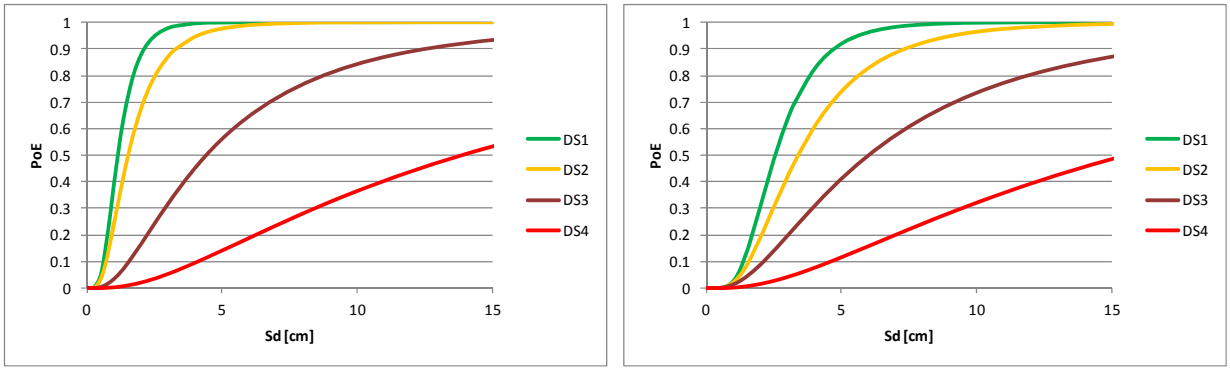

Figure 19. Fragility curves with the definition of damage states Equation 11 for: (a) 1st_fix, (b) 1st_ssi, and with the definition Equation 12 for: (d) 1st_fix, (d) 1st_ssi.

Table 5 summarizes the mean values of spectral displacements for each defined damage state and for each studied building typology (columns 1 to 6). Also given in the table are the values of lognormal mean μ and standard deviation β (columns 7 and 8). This standard deviation can be assumed that corresponds to the uncertainty due to the definition of the damage states $\beta_{T,ds,i}$.

Table 5. Spectral displacements of damage thresholds for the damage states.

	3st_fix	3st_ssi	2st_fix	2st_ssi	1st_fix	1st_ssi	μ	β
	1	**2**	**3**	**4**	**5**	**6**	**7**	**8**
DS1	0.49	2.89	0.32	1.79	0.89	1.98	1.39	0.79
DS2	3.49	3.47	0.83	2.46	1.27	2.83	2.39	0.75
DS3	7.98	4.34	1.60	3.47	4.72	6.00	4.69	0.74
DS4	20.87	29.99	20.63	24.99	15.09	15.53	21.18	0.71

Assuming that β_D (variability in the ground motion) and β_C (variability in the resistance of the structure) have a value 0.7 and combining (through SRSS) with the mean values of $\beta_{T,ds,i}$ from **Table 5**, a general set of fragility curves for timber-framed masonry buildings is generated that could be used for all TFM categories (**Figure 20**).

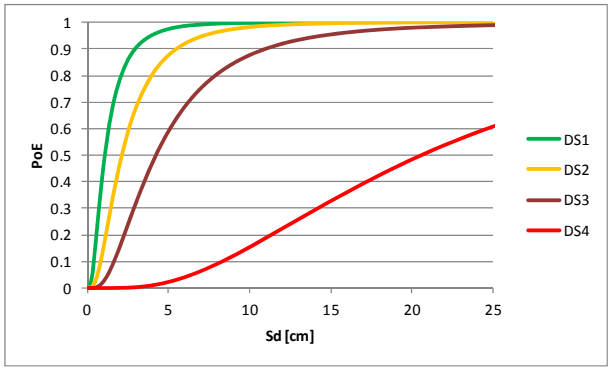

Figure 20. General fragility curves for timber-framed masonry buildings.

3.2.1 Fragility curves in terms of PGA

Fragility curves in terms of PGA can be derived with the aid of analysis of typical structures for a gradually increasing intensity (incremental dynamic analysis); nonlinear response-history analyses are carried out for various ground motions (accelerograms) and then, capacity curve are drawn in terms of PGA encompassing the variability of the records (Vamvatsikos and Cornell 2002). An alternative to this rigorous, yet cumbersome, procedure is applied herein and consists in converting the spectral displacement values defining the damage state thresholds into PGA values using a suitable response spectrum; of course, the so-derived curves are now specific to the selected ground motion (unlike the curves in terms of S_d). A convenient method is the N2 procedure (Fajfar 1999; Fajfar 2000) based on the assumption of equal elastic and inelastic displacements in the medium to long period range**.**

Table 6. Mean damage states thresholds in PGA [g].

state	3st_fix_fix	3 st_fix_ssi	2 st_fix_fix	2 st_fix_ssi	1 st_fix_fix	1 st_fix_ssi
	1	2	3	4	5	6
DS1	0.1	0.21	0.11	0.13	0.14	0.21
DS2	0.27	0.25	0.14	0.18	0.2	0.31
DS3	0.58	0.32	0.15	0.25	0.4	0.46
DS4	1.52	2.18	1.51	1.83	1.1	1.14

The damage state thresholds defined in terms of S_d in **Table 5** are converted into PGA values using the 5%-damped response spectrum of EC-8 (CEN 2004b) for soil category D, as this reasonably matches the soil conditions in the city of Lefkas. The damage thresholds are given in Table 6 and fragility curves for the studied building typologies (Table 2) are shown in Figure 21; the standard deviations β are assumed to be the same as previously.

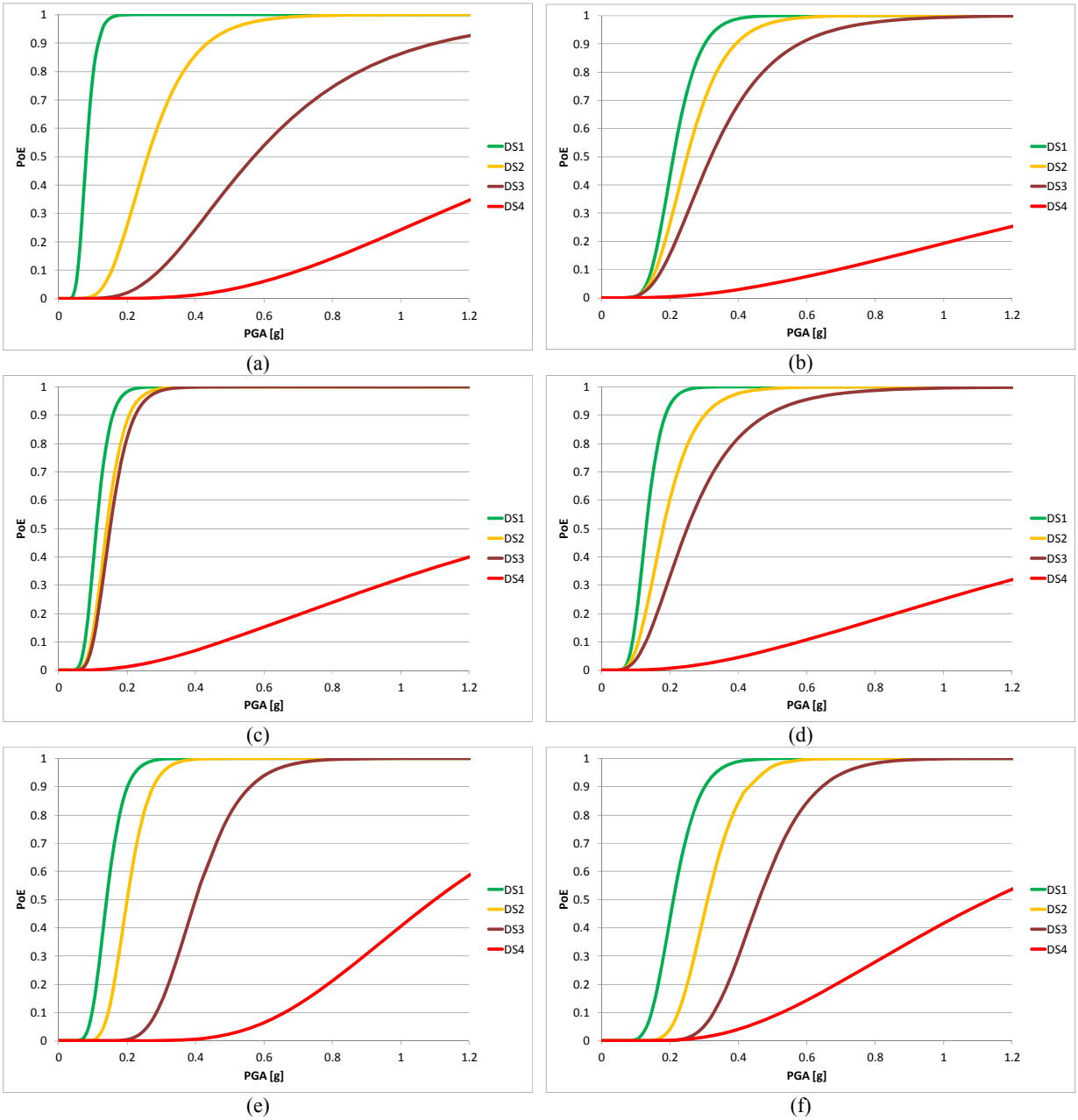

Figure 21. Fragility curves in terms of PGA for the following building typologies: (a) 3st_fix, (b) 3st_ssi, (c) 2st_fix, (d) 2st_ssi, (e) 1st_fix and (f) 1st_ssi.

The herein analytically generated fragility curves are compared with the empirical fragility curves proposed by Karababa (2007); Karababa and Pomonis (2011), which are in terms of the 'parameterless' intensity ψ. This ψ intensity, initially proposed by Spence et al. (1991), assumes an arbitrary value of 10 when 50% of the masonry building stock exceeds the damage state DS3 (Table 3), i.e. ψ=10 is the threshold of DS3. The key assumption -justified empirically- is that buildings belonging to one typology will be distributed similarly among

the various damage grades when submitted to similar ground motions. The following equation is proposed (Pomonis et al. 1992) to convert the parameterless intensity ψ into PGA (cm/s^2):

$$\log PGA = 2.034 + 0.054\psi \tag{11}$$

The mean values of the damage state thresholds in the parameterless ψ intensity and in PGA are presented in the following **Table 7**. In this table the acronym 'LBSM & TF' stands for dual load-bearing timber-framed stone masonry structures, while 'TF' for pure timber-framed structures.

Table 7. Mean damage state thresholds by (Karababa and Pomonis 2011).

DS	LBSM & TF		TF	
	ψ	PGA [g]	ψ	PGA [g]
DS1	3.7	0.17	8.5	0.32
DS2	8.4	0.31	9.4	0.35
DS3	10.5	0.41	11.2	0.44
DS4	12.6	0.53	14.3	0.65
DS5	13.7	0.61	15.5	0.76

Comparing the analytically generated fragility curves (Table 6) with the empirical ones (Table 7), it is seen that the mean values of the damage state thresholds are very close for the first three damage states. Averaging the mean values of Table 6 for the various typologies (average of each row of the columns 1 to 6) results in 0.15g for damage state DS1, 0.23g for damage state DS2, 0.36g for damage state DS3, and 1.55g for damage state DS4. However, there is a large discrepancy for damage state DS4. This should be attributed to various reasons: First that during the Lefkas 2003 earthquake there were no timber-framed buildings that experienced a collapse damage state DS4 (Karababa and Pomonis define DS4 as 'Very severe to partial collapse', and DS as Total Collapse, these two DS are treated as one in the analytically derived curves), and thus, extrapolating the empirical data to not observed damage states entails high uncertainty. Second, the code response spectrum used to convert the S_d values to PGA may not be representative for all the examined region. Moreover, the empirical Equation 11 used for converting the parameterless intensity ψ to PGA is characterised (like all similar equations) by high dispersion. However, both analyses lead to the conclusion that timber-framed buildings can resist without collapse very strong earthquakes. Further empirical data are needed, to enhance the current database. The comparison for the pure timber-framed buildings shows that the analytically generated fragility curves are less conservative. Besides the previous sources of dispersion, one should also point out the small statistical sample that comprised only 577 buildings. Given the variability inherent in such analyses, the match of the analytical and the empirical curves is reasonably good.

4. PILOT SEISMIC LOSS SCENARIO

The fragility curves derived for timber-framed masonry structures in §3 are used here to carry out a seismic loss assessment for the city of Lefkas subjected to the 2003 earthquake. The results of the post-event survey conducted by the Departments for Seismic Restoration (TAS) in the municipalities of the island were processed by Karababa (2007) to provide the statistical data summarized in **Table 8.** It is important to note that the TAS groups visited only the buildings wherein they were invited by the owners or tenants. A key assumption made by Karababa (2007) is that buildings not visited by the survey groups had no damage. No indication is given as to whether a verification of this assumption was made by field work, and it is possible that there are cases wherein this assumption might not be valid since the groups may not have been invited for reasons such as the absence of the owner or unwillingness of the owners that feared possible drop in the value of their property if damage to the building was documented (e.g. yellow tag).

The estimation of the seismic intensity in Karababa and Pomonis (2011) is based on the attenuation relationship proposed by Skarlatoudis et al. (2003) for the Greek territory. As already noted, the parameterless ψ intensity has to be converted to PGA using empirical relationships (such as Equation 11), so the entire process is subject to significant uncertainty.

Table 8. Distribution of damage in the Lefkas city for seismic intensity I_{MM}=7.11.

	RC		URM		TF	
	building number	%	building number	%	building number	%
DS0	1624	80.20%	281	50.10%	516	56.80%
DS1	230	11.40%	92	16.40%	183	20.10%
DS2	119	5.90%	86	15.30%	142	15.60%
DS3	46	2.30%	51	9.10%	55	6.10%
DS4	6	0.30%	51	9.10%	13	1.40%
DS5	0	-	0	-	0	-

In the present loss assessment the distribution of intensity provided by the shake map of USGS (2003) is adopted; according to this map the city of Lefkas experienced a PGA of 0.19g. Inserting this PGA to the fragility curves of **Figure 21** the losses reported in **Table 9** were estimated. In this table column 3 gives the number of damaged TFM buildings according to the in-situ post-earthquake inspection and column 4 the percentage assigned to each DS. Column 11 is the average percentage for the various TFM classes from the analysis (columns 5 to 10). Comparing the latter with column 4 (referring to the entire TFM stock) a good overall match is observed, but there are significant discrepancies for some categories. The mean damage factor (MDF) in column 2, which is a representative damage indicator, shows good correlation with the empirical data.

Table 9. Scenario of loss estimation for the Lefkas 2003 earthquake and the empirical data.

	MDF	TF	%	3fix_fix	3fix_ssi	2fix_fix	2fix_ssi	1fix_fix	1fix_ssi	μ
1	2	3	4	5	6	7	8	9	10	11
DS0	0	516	56.80	1.00%	62.20%	2.40%	100.00%	13.10%	62.20%	48.00%
DS1	0.05	183	20.10	79.00%	14.90%	12.30%	0.00%	43.10%	34.90%	21.00%
DS2	0.2	142	15.60	18.40%	9.30%	6.60%	0.00%	43.60%	2.90%	12.50%
DS3	0.45	55	6.10	1.50%	13.20%	77.50%	0.00%	0.30%	0.10%	18.20%
DS4	0.8	13	1.40	0.00%	0.30%	1.10%	0.00%	0.00%	0.20%	0.30%
MDF			8.00	8.30%	8.80%	37.70%	0.00%	11.00%	2.50%	12.00%
Σ		909	100	100%	100%	100%	100%	100%	100%	100%

5. CONCLUSIONS

Timber-framed masonry buildings in Lefkas that have a dual structural system (described in section 2) can be thought of as an early realisation of displacement based 'design', as they were found to resist strong earthquakes through their displacement capacity rather than their strength. The primary (URM) system aims to support gravity loads and, under low to moderate intensity earthquakes, to prevent damage and noticeable deflection of the building. On the other hand, the secondary (timber frame) system renders displacement capacity to the building and hence the necessary deformability to survive a severe seismic event.

The study of TFM buildings at the phases wherein the above two systems (primary and secondary) are active was performed using a different model for each; this is a pragmatic analysis procedure since the presence of the secondary system has a negligible effect on the response when the primary system is still intact. Pushover curves of timber-framed masonry buildings with a dual system are best idealised by a quadri-linear curve representing the transition of the building through four discrete response stages.

Damage states were related to the response phases of the building, defined in terms of displacements. So, three (DS1, DS3 and DS4) out of the four damage states are related directly to the response phases, establishing a robust definition that facilitates damage classification during post-earthquake surveys and inspections.

The derived fragility curves for TFM buildings are in terms of spectral displacement; they are also recast in terms of PGA correlating the latter to S_d on the basis of a response spectrum. They show that although timber-framed masonry structures may suffer cracks and damage for low intensity earthquakes, they are expected to avoid collapse due to their high displacement capacity. These findings agree with observed response of the buildings in the 2003 earthquake in Lefkas. The comparison with the empirical curves showed reasonable match.

A loss estimation scenario was developed for TFM buildings in the city of Lefkas subjected to the 2003 earthquake. The key comparison with observed damage data was made for the entire TFM stock (rather than the various sub-classes used in the fragility analysis) and showed good match for most of the damage states.

Acknowledgments

The author L.A. Kouris gratefully acknowledges the financial support provided by the Aristotle University of Thessaloniki (Grant 16046/2011) for carrying out this work.

References

Apostolopoulos C, Sotiropoulos P (2008) Venetian churches of Lefkada, Greece Construction documentation and seismic behaviour "Virgin Mary of the Strangers". Constr Build Mater 22: 434-443.10.1016/j.conbuildmat.2006.10.016

Barbat AH, Pujades LG, Lantada N (2008) Seismic damage evaluation in urban areas using the capacity spectrum method: Application to Barcelona. Soil Dyn Earthqu Eng 28: 851-865.10.1016/j.soildyn.2007.10.006

Copani P (2007) Timber-Frame Buildings in Scandinavia: High Deformation Prevent the System from Collapse. ICOMOS IWC - XVI International Symposium: From Material to Structure - Mechanical Behaviour and Failures of the Timber Structures, 11th -16th November, Florence, Venice and Vicenza, Italy.

De Jong B, Keijsers JG, Riksen MJ, Krol J, Slim PA (2014) Soft Engineering vs. a Dynamic Approach in Coastal Dune Management: A Case Study on the North Sea Barrier Island of Ameland, The Netherlands. J Coast Res: http://dx.doi.org/10.2112/JCOASTRES-D-13-00125.1

CEN [Comité Européen de Normalisation] (2004a), Eurocode 5: Design of timber structures Part 1-1: General — Common rules and rules for buildings (EN 1995-1-1: 2004), Brussels, Dec. 2004.

CEN [Comité Européen de Normalisation] (2004b), Eurocode 8: Design of structures for earthquake resistance—Part 1: General rules, seismic actions and rules for buildings, Brussels, Dec. 2004.

CEN (2005), "Eurocode 8: Design of Structures for Earthquake Resistance - Part 3: Assessment and retrofitting of buildings", (EN 1998-3:2005), Brussels, March 2005.

Computers and Structures Inc., SAP2000: Three dimensional static and dynamic finite element analysis and design of structures, Berkeley, California, 1999.

Fajfar P (1999) Capacity spectrum method based on inelastic demand spectra. Earthquake engineering and structural dynamics 28: 979-994.

Fajfar P (2000) A Nonlinear Analysis Method for Performance-Based Seismic Design. Earthquake Spectra 16: 573-592.

FEMA [Federal Emergency Management Agency] (2000) Prestandard and commentary for the seismic rehabilitation of buildings. Report FEMA-356, Washington, DC.

Freeman S (1998) Development and use of capacity spectrum method. 6th US-NCEE Conference on Earthquake Engineering/EERI, May 31 - June 4, Seattle, Washington, paper No. 269.

Hendry AW (1998) *Structural masonry.* Macmillan Press

Hill M, Rossetto T (2008) Comparison of building damage scales and damage descriptions for use in earthquake loss modelling in Europe. Bulletin of Earthquake Engineering 6: 335-365.

Indirli M, Kouris LAS, Formisano A, Borg RP, Mazzolani FM (2013) Seismic damage assessment of unreinforced masonry structures after the Abruzzo 2009 earthquake: The case study of the historical centers of L'Aquila and Castelvecchio Subequo. Int J Archit Herit 7: 536-578.10.1080/15583058.2011.654050

Kappos AJ, Stefanidou S (2010) A deformation-based seismic design method for 3D R/C irregular buildings using inelastic dynamic analysis. Bulletin of earthquake engineering 8: 875-895.

Kappos AJ, Kouris LA (2008) Modelling of Traditional Masonry Timber Framed Structures. 3rd National Conference of Earthquake Engineering, November 5th-7th, Athens, Greece, paper No. 2013 [in Greek].

Kappos AJ, Panagopoulos G, Panagiotopoulos C, Penelis G (2006) A hybrid method for the vulnerability assessment of R/C and URM buildings. Bull Earthquake Engin 4: 391-413.10.1007/s10518-006-9023-0

Kappos, A.J., G.K. Panagopoulos, A.G. Sextos, V.K. Papanikolaou, K.C. Stylianidis (2010) Development of Comprehensive Earthquake Loss Scenarios for a Greek and a Turkish City - Structural Aspects. Earthquakes & Structures 1(2): 197-214.

Kappos AJ, Penelis GG, Drakopoulos CG (2002) Evaluation of simplified models for lateral load analysis of unreinforced masonry buildings. J Struct Eng 128: 890-897.10.1061/(ASCE)0733-9445(2002)128:7(890).

Karababa FS, Guthrie PM (2007) Vulnerability Reduction through Local Seismic Culture. Technology and Society Magazine, IEEE 26: 30-41.

Karababa FS (2007) Local seismic construction practices as a means to vulnerability reduction and sustainable development. The case-study of Lefkada Island. PhD Thesis, University of Cambridge.

Karababa FS, Pomonis A (2011) Damage data analysis and vulnerability estimation following the August 14, 2003 Lefkada Island, Greece, Earthquake. Bulletin of Earthquake Engineering 9: 1015-1046.

Karakostas C, Lekidis V, Makarios T, Salonikios T, Sous I, Demosthenous M (2005) Seismic response of structures and infrastructure facilities during the Lefkada, Greece earthquake of 14/8/2003. Eng Struct 27: 213-227.10.1016/j.engstruct.2004.09.009

Kircher CA, Whitman RV, Holmes WT (2006) HAZUS earthquake loss estimation methods. Nat Hazards Rev 7: 45.

Kouris LA, Kappos A Seismic performance of ancient timber-framed walls. 4th International Congress: Science and Technology for the Safeguard of Cultural Heritage of the Mediterranean Basin, in: A. Ferrari (Ed.), Cairo, Egypt, December 6th - 8th, vol I, pp. 119-127.

Kouris LAS (2012) Assessment of the seismic behaviour of timber-framed masonry buildings. PhD Thesis, Department of Civil Engineering, Aristotle University of Thessaloniki). Available in: http://phdtheses.ekt.gr/eadd/handle/10442/29305 [in Greek].

Kouris LA, Borg RP, Indirli M (2010) The L'Aquila earthquake, April 6th, 2009: A review of seismic damage mechanisms. COST ACTION C26: Urban Habitat Constructions under Catastrophic Events - Proceedings of the Final Conference, in: F. Mazzolani (Ed.), Taylor & Francis Group, London, pp. 673-681, ISBN: 978-0-415-60685-1, 16-18 September, Naples, Italy..

Kouris LAS (2013) Practical simulation tools for the seismic analysis of Timber-Framed masonry structures. Proceedings of the 1st International Symposium on Historic Earthquake-Resistant Timber Frames in the Mediterranean Region H.Ea.R.T. November 4th-5th, Cosenza, Italy.

Kouris LAS, Kappos AJ (2014) A practice-oriented model for pushover analysis of a class of timber-framed masonry buildings. Eng Struct 75: 489-506.

Kouris LAS, Kappos AJ (2012) Detailed and simplified non-linear models for timber-framed masonry structures. J Cult Heritage 13: 47-58.10.1016/j.culher.2011.05.009

Kouris LAS, Meireles H, Bento R, Kappos AJ (2014) Simple and complex modelling of timber-framed masonry walls in Pombalino buildings. Bulletin of Earthquake Engineering: 1-27.10.1007/s10518-014-9586-0

Kowalsky MJ, Priestley MJN, MacRae GA (1995) Displacement-based design of RC bridge columns in seismic regions. Earthquake Eng Struct Dyn 24: 1623-1643.10.1002/eqe.4290241206

Lagomarsino S (2006) On the vulnerability assessment of monumental buildings. Bull Earthquake Engin 4: 445-463.10.1007/s10518-006-9025-y

Makarios T, Demosthenous M (2006) Seismic response of traditional buildings of Lefkas Island, Greece. Eng Struct 28: 264-278.10.1016/j.engstruct.2005.08.002

Moehle JP (1992) Displacement ‐ Based Design of RC Structures Subjected to Earthquakes. Earthquake Spectra 8: 403-428.10.1193/1.1585688

Naraine K, Sinha S (1991) Cyclic Behavior of Brick Masonry Under Biaxial Compression. Journal of Structural Engineering-Asce 117: 1336-1355.

Panagopoulos G, Kappos AJ. Bilinear approximation of force-deformation curves. 16th Hellenic Conference of Reinforced Concrete. Paphos, Cyprus, October 21-23, 2009 [in Greek].

Papazachos V, Papazachos B, Papazachou C, & Papazachou K (1997) *The earthquakes of Greece.* Editions Ziti

Penelis GG (2006) An efficient approach for pushover analysis of unreinforced masonry (URM) structures. J Earthqu Eng 10: 359-379.10.1142/S136324690600258X

Pomonis A, Coburn AW, Spence RJS (1992) Strong Ground Motion and Damage to Masonry Buildings As Revealed By Damage Surveys Near Recording Instruments. Martin Centre Publication, Cambridge.

Porphyrios DTG (1971) Traditional Earthquake-Resistant Construction on a Greek Island. The Journal of the Society of Architectural Historians 30: 31-39.

Pujades LG, Barbat AH, González-Drigo R, Avila J, Lagomarsino S (2010) Seismic performance of a block of buildings representative of the typical construction in the Eixample district in Barcelona (Spain). Bull Earthquake Engin: 1-19.10.1007/s10518-010-9207-5

Rondoyanni T, Sakellariou M, Baskoutas J, Christodoulou N (2012) Evaluation of active faulting and earthquake secondary effects in Lefkada Island, Ionian Sea, Greece: An overview. Nat Hazards 61: 843-860.

Rossetto T, Kappos AJ, Kouris LA, Indirli M, Borg RP, Lloyd TO, Sword-Daniels V (2010) Comparison of damage assessment methodologies for different natural hazards. COST ACTION C26: Urban Habitat Constructions under Catastrophic Events - Proceedings of the Final Conference, in: F. Mazzolani (Ed.), Taylor & Francis Group, London, pp. 1023-1029, ISBN: 978-0-415-60685-1, 16-18 September, Naples, Italy..

Skarlatoudis A, Papazachos C, Margaris B, Theodulidis N, Papaioannou C, Kalogeras I, Scordilis E, Karakostas V (2003) Empirical peak ground-motion predictive relations for shallow earthquakes in Greece. Bulletin of the Seismological Society of America 93: 2591-2603.

Spence R, Coburn A, Sakai S, Pomonis A (1991) A parameterless scale of seismic intensity for use in seismic risk analysis and vulnerability assessment. Proceedings of International Conference in Earthquake Blast and Impact: Measurement and effects of vibration, Manchester, U.K.

Stamatelos IN (1870) The 13 reported catastrophes of the Lefkas Island from 1612 until 1869, Ephimeris Philomathon, No. 726, yr 18, p. 1985, Athens [in Greek].

Touliatos P, Gante D (1995) *Local traditional earthquake-resistant construction: the paradigm of Lefkas*, National Technical University of Athens, Athens [in Greek].

US Geological Survey [USGS] (2003) Magnitude 6.3 Greece August 14, 2003; available at http://earthquake.usgs.gov/earthquakes/eqarchives/year/2003/2003_08_14.php.

United Nations (1993) The traditional aseismic techniques and the everlasting principles they reveal. Newsletter - Stop Disasters. International decade for natural disasters reduction "Seismic Vulnerability Reduction": 4-5.

Vamvatsikos D, Nigro E, Kouris L, Panagopoulos G, Kappos A, Rossetto T, Lloyd T, Stathopoulos T (2010a) Performance assessment under multiple hazards. Urban Habitat Constructions under Catastrophic Events, in: F. Mazzolani (Ed.), Taylor & Francis Group, London, pp. 271-289, ISBN: 978-0-415-60686-8.

Vamvatsikos D, Cornell CA (2002) Incremental dynamic analysis. Earthquake Eng Struct Dyn 31: 491-514.

Vamvatsikos D, Kouris LA, Panagopoulos G, Kappos AJ, Nigro E, Rossetto T, Lloyd TO, Stathopoulos T (2010b) Structural vulnerability assessment under natural hazards: A review. COST ACTION C26: Urban Habitat Constructions under Catastrophic Events - Proceedings of the Final Conference, in: F. Mazzolani (Ed.), Taylor & Francis Group, London, pp. 711-723, ISBN: 978-0-415-60685-1, 16-18 September, Naples, Italy.

Vieux-Champagne F, Sieffert Y, Grange S, Polastri A, Ceccotti A, Daudeville L (2014) Experimental analysis of seismic resistance of timber-framed structures with stones and earth infill. Eng Struct 69: 102-115.http://dx.doi.org/10.1016/j.engstruct.2014.02.020

Vintzileou E (2011) Timber-reinforced structures in Greece: 2500 BC-1900 AD. Proceedings of the Institution of Civil Engineers.Structures and buildings 164: 167-180.

Vintzileou E, Touliatos P (2005) Seismic behaviour of the historical structural system of the island of Lefkada, Greece. Advances in Architecture Series 20: 291-300.

Vintzileou E, Zagkotsis A, Repapis C, Zeris C (2007) Seismic behaviour of the historical structural system of the island of Lefkada, Greece. Constr Build Mater 21: 225-236.10.1016/j.conbuildmat.2005.04.002

Whitman RV, Anagnos T, Kircher CA, Lagorio HJ, Lawson RS, Schneider P (1997) Development of a national earthquake loss estimation methodology. Earthquake Spectra 13: 643-661.